Proc. Natl. Acad. Sci. USA
Vol. 89, pp. 3610–3614, April 1992
Biophysics

Reversible steps in the bacteriorhodopsin photocycle

(absorption spectroscopy/kinetics/global modeling)

RICHARD H. LOZIER*, AIHUA XIE†, JAMES HOFRICHTER*, AND G. MARIUS CLORE*

*Laboratory of Chemical Physics, National Institutes of Diabetes, Digestive, and Kidney Diseases, National Institutes of Health, Bethesda, MD 20892; and †Department of Physics, University of Illinois at Urbana Champaign, Urbana, IL 61801

Communicated by William A. Hagins, November 27, 1991 (received for review June 1, 1991)

ABSTRACT **The absorbance changes that accompany the light-driven proton-pumping cycle of bacteriorhodopsin measured over a broad range of times, wavelengths, temperatures, and pH values have been globally fitted to the kinetic model $K \rightleftharpoons L \rightleftharpoons X \rightleftharpoons M \rightleftharpoons N \rightleftharpoons O \rightarrow bR$. A remarkably good fit to the data was obtained by optimizing the rate constants at 20°C and the corresponding activation energies at each pH value, together with the extinction coefficients for each intermediate, which were assumed to be independent of both pH and temperature. Back-reactions are included for all but the last step of the cycle and are found to be essential for fitting the data. The rates of these reactions are large, and the analogous irreversible model produced significantly worse fits to the data. Small systematic differences between the fit and the experimental data associated with the X, M, and O intermediates, together with the inability of the model to produce spectra for the X and M intermediates consistent with their assignment as molecular species, indicate that this model must be an incomplete description of the photocycle. We suggest that these problems arise from the presence of additional occupied states that are difficult to distinguish on the basis of their visible absorption spectra alone.**

Bacteriorhodopsin (bR) is a retinylidene protein present in "purple membrane" patches in the plasma membrane of *Halobacterium halobium*. It functions as a light-driven proton pump, converting solar energy to biochemical energy in the form of a pH gradient and electrochemical potential across the membrane (1–3). The pumping cycle is initiated and energized by the absorption of a photon by the "light-adapted" state of bR, in which the retinal chromophore is in the all-trans conformation, and concludes by returning the molecule to the same state. The photocycle of bR was first studied by monitoring light-induced absorbance changes and was modeled as an unbranched unidirectional cycle with four (or five) intermediates (4):

$$bR \xrightarrow{h\nu} K \rightarrow L \rightarrow M \rightarrow (N) \rightarrow O \rightarrow bR. \qquad [1]$$

The N state has since been characterized in experiments at high pH and salt concentrations (5, 6). Studies using a variety of spectroscopic and electrochemical techniques have suggested a variety of additional intermediates in the photocycle, including X (7), situated between L and M; additional L (8, 9) and M (8–11) intermediates; as well as additional intermediates in the later portion of the photocycle. With few exceptions (12, 13), the contribution of back-reactions has been ignored until recently. Ames and Mathies (14) have used a reversible-sequential model with four intermediates to fit time-resolved resonance Raman data obtained under high salt conditions, and Varo, Lanyi, and coworkers (15–17) have used models having six intermediate states, which include both reversible and irreversible steps to fit time-resolved absorption data.

To explore the accuracy with which sequential models can describe the proton-pumping cycle for wild-type bR, we have used a global fitting approach in which the number of input assumptions is minimized to reexamine such models for the bR photocycle. To date, most kinetic data on the bR photocycle have either been interpreted qualitatively or have been analyzed in terms of a sum of n exponential relaxations. The relaxation rates and amplitudes obtained from such an analysis are determined by the intrinsic rate constants of a kinetic model but, because all n-intermediate first-order models have the same general solution, this approach is of limited utility for elucidating reaction pathways and obtaining insight into the nature of intermediate species. To carry out the present analysis, a kinetic model is postulated by specifying the set of intermediates and rates that describe the kinetic pathway. The differential equations that describe the model are numerically integrated, and the resulting solution is optimized by adjusting the unknown parameters. To impose as high a level of constraint as possible on the models, we have used a data set that covers a broad range of times and experimental conditions. As pointed out previously (18, 19), these features of the data are *essential* in discriminating among potential kinetic models. The criteria for selection of an acceptable model are that it must have a standard deviation comparable to the standard error of the data and exhibit good determination of physically reasonable values for the optimized parameters.

METHODS

We have analyzed the data of Xie *et al.* (20), which describe absorbance changes of aqueous suspensions of purple membrane at three pH values (5, 7, and 9), in a total salt concentration of 0.01 M, and at seven temperatures ranging from 5°C to 35°C. Data were collected from 1 μs until completion of the photocycle following excitation by a 10-ns 490-nm laser flash. Measuring wavelengths were 420, 540, 600, and 660 nm, where the transient absorbance changes are large and representative of specific intermediates, at 5, 15, 25, and 35°C and these four plus 11 additional wavelengths from 380 to 700 nm at 10, 20, and 30°C. The data set at each pH thus consists of 61 kinetic traces, each of which describes the absorbance changes at 47 time points, equally spaced on a logarithmic scale from 1 μsec to 300 msec (i.e., a total of 183 vectors and 8601 data points).

The data were fitted simultaneously to kinetic models by using the program FACSIMILE, which is a package for the automatic solution of initial value problems arising as systems of differential equations (19, 21). To simultaneously fit the data at the different times, wavelengths, temperatures, and pH values, the following parameters were optimized: (*i*) the rate constants at 20°C and the corresponding Arrhenius

The publication costs of this article were defrayed in part by page charge payment. This article must therefore be hereby marked "*advertisement*" in accordance with 18 U.S.C. §1734 solely to indicate this fact.

Abbreviation: bR, bacteriorhodopsin.

activation energies for each step in a proposed model: the rate constants at the other temperatures are then calculated using a simple Arrhenius relationship

$$k(T_j) = k(T_0)e^{E_A(1/RT_0 - 1/RT_j)}, \quad [2]$$

where $k(T_0)$ is the rate constant at the reference temperature (T_0 = 293.15 K), $k(T_j)$ is the rate constant at temperature T_j, E_A is the temperature-independent activation energy, and R is the gas constant, (*ii*) the *temperature-* and *pH-independent* differential extinction coefficients for each intermediate at each wavelength (relative to the starting species, bR), and (*iii*) a factor that scales the amplitude of the kinetic curve measured at each pH, temperature, and wavelength to correct for variations in the intensity of the actinic flash. The resulting number of parameters is large, but the richness of the kinetic data allows nearly all of these parameters to be well determined.

RESULTS AND DISCUSSION

Preliminary fitting was carried out to test a variety of unbranched reversible models by using subsets of the data. Fits to the data at each individual pH using the model A ⇌ B ⇌ C ⇌ D → bR yielded residuals that were <1% of the maximum data amplitudes and the following conclusions. The first three intermediates, A, B, and C, have similar difference spectra at each pH value and can be identified with the K, L, and M intermediates, respectively (4). Intermediate D is similar at pH 5 and 7 and is characteristic of the O intermediate (4), whereas the spectrum of D is clearly different at pH 9 and can be assigned to intermediate N (5). Setting the back-reaction rates to zero resulted in substantially worse fits. In fact, at pH 5 and pH 7, including the reverse reactions in this model improved the fit more than expanding the irreversible model to include an additional intermediate. To test the possibility that branch reactions (e.g., a bypass pathway from C to bR) might improve the fits of the four-species model, we attempted to fit the pH 5 subset of the data by using various branched models. In each case, the rate constant for the proposed branch was poorly determined, indicating that the data provide no evidence for such schemes.

From these results it appeared that the complete data set might be fitted by incorporating both the N and O intermediates in a sequential pathway. Accordingly, we fitted the combined data at pH 5, 7, and 9 to the model K ⇌ L ⇌ M ⇌ N ⇌ O → bR. The kinetic and spectral parameters of this model were well determined, but the fit showed significant systematic residuals in the 1- to 100-μsec time range at all pH values. We therefore proceeded to fit the full data set to the six-intermediate model

$$K \rightleftharpoons L \rightleftharpoons X \rightleftharpoons M \rightleftharpoons N \rightleftharpoons O \rightarrow bR, \quad [3]$$

which yielded a fit comparable in quality to those obtained for the separate pH subsets of the data using the four-intermediate model. It is important to note that, since no assumptions or constraints were imposed on the difference spectra of the intermediate species, the spectra produced by FACSIMILE are determined *only* by their ability to fit the data. The best-fit values for the rate constants and activation energies are given in Table 1.

Fig. 1 shows a comparison of the experimental data at four selected wavelengths with the best-fit curves obtained using this model (Eq. **3**). The standard deviation of the fit (4.1×10^{-4} absorbance units) is comparable to the experimental errors in the data. There are, however, systematic differences between the data and the fit with amplitudes up to about 10^{-3} absorbance units. The largest deviations occur at the highest temperatures in the kinetics of formation of the red-shifted O intermediate. Specifically, the experimental data at 660 nm rise more steeply than the fit in the millisecond time range at all pH values. Small systematic deviations also remain in the 100-μsec time range at pH 9, which have not been removed by addition of the X intermediate.

The time-dependent concentrations of the seven species of the six-intermediate model (Eq. **3**) are shown in Fig. 2. The early steps of the photocycle exhibit similar kinetics at all pH values, and the reverse rates for almost all of the early steps in the cycle are significant. A small amount of the K intermediate (about 7% at 20°C) persists throughout the lifetime of L. The L and X intermediates are also present as a mixture at all pH values. The model interprets the fast rise of the absorbance in the blue region of the spectrum at high pH (22) as resulting from the formation of X, which has significant extinction between 380 and 440 nm (see Fig. 3) and hence must contain some deprotonated 13-*cis*-retinal. As a result of the X ← M back-reaction, the intermediate X also persists throughout the lifetime of the M intermediate at pH 5 and pH 9. At pH 7, the fitted value for the X ← M rate is effectively zero, resulting in the highest maximal M concentration at all temperatures.

As anticipated from the independent fits at the three pH values described above, the decay of the M intermediate, via

Table 1. Rate constants and activation energies obtained from fits of the model K ⇌ L ⇌ X ⇌ M ⇌ N ⇌ O → bR (Eq. **3**)

	pH 5		pH 7		pH 9	
Reaction	k (20°C)	E_A	k (20°C)	E_A	k (20°C)	E_A
Forward						
K → L	$5.42 \pm 0.10 \times 10^5$	9.0 ± 0.3	$5.38 \pm 0.09 \times 10^5$	8.9 ± 2.7	$5.97 \pm 0.11 \times 10^5$	8.9 ± 0.3
L → X	$2.46 \pm 0.06 \times 10^4$	17.7 ± 0.4	$5.03 \pm 0.78 \times 10^4$	12.6 ± 1.9	$9.60 \pm 0.55 \times 10^4$	17.6 ± 1.0
X → M	$1.14 \pm 0.14 \times 10^4$	15.3 ± 1.7	$6.42 \pm 1.2 \times 10^4$	10.3 ± 1.9	$1.93 \pm 0.10 \times 10^4$	12.1 ± 0.8
M → N	$1.69 \pm 0.18 \times 10^2$	16.4 ± 1.2	$1.79 \pm 0.47 \times 10^3$	6.1 ± 1.9	$2.54 \pm 0.04 \times 10^2$	19.7 ± 0.2
N → O	$3.68 \pm 1.60 \times 10^3$	13.5 ± 5.7	$1.69 \pm 0.12 \times 10^3$	29.5 ± 1.0	71.5 ± 45	18.0 ± 9.1
O → bR	$1.33 \pm 0.03 \times 10^2$	5.9 ± 0.4	$2.57 \pm 0.06 \times 10^2$	7.5 ± 0.5	$5.06 \pm 7.6 \times 10^2$	0.8 ± 3.2
Reverse						
K ← L	$4.14 \pm 0.35 \times 10^4$	21.8 ± 1.3	$3.68 \pm 0.34 \times 10^3$	22.6 ± 1.4	$5.70 \pm 0.44 \times 10^3$	21.5 ± 1.1
L ← X	$1.26 \pm 0.25 \times 10^3$	15.7 ± 2.9	$2.16 \pm 0.79 \times 10^4$	−7.4 ± 3.0	$1.48 \pm 0.16 \times 10^4$	10.2 ± 1.8
X ← M	$3.00 \pm 0.14 \times 10^3$	8.3 ± 0.8	*	*	$1.58 \pm 0.07 \times 10^3$	12.3 ± 0.7
M ← N	$5.43 \pm 2.8 \times 10^2$	29.1 ± 3.9	$1.61 \pm 0.51 \times 10^4$	16.0 ± 2.0	20.5 ± 3.5	30.2 ± 2.4
N ← O	$1.62 \pm 1.2 \times 10^2$	(−13.8) ± 5.1	27.4 ± 7.1	6.8 ± 5.1	$5.26 \pm 6.8 \times 10^2$	0.7 ± 17.6

Errors are reported as the 5%–95% confidence limits from the final iteration of the fit. Trial calculations using subsets of the data suggest that these values are, in most cases, reasonable estimates of the actual errors.

*Parameters not optimized in the final fit because they were found in the initial fitting stages to be ill-determined by the data. The value selected prior to discarding this parameter was effectively zero.

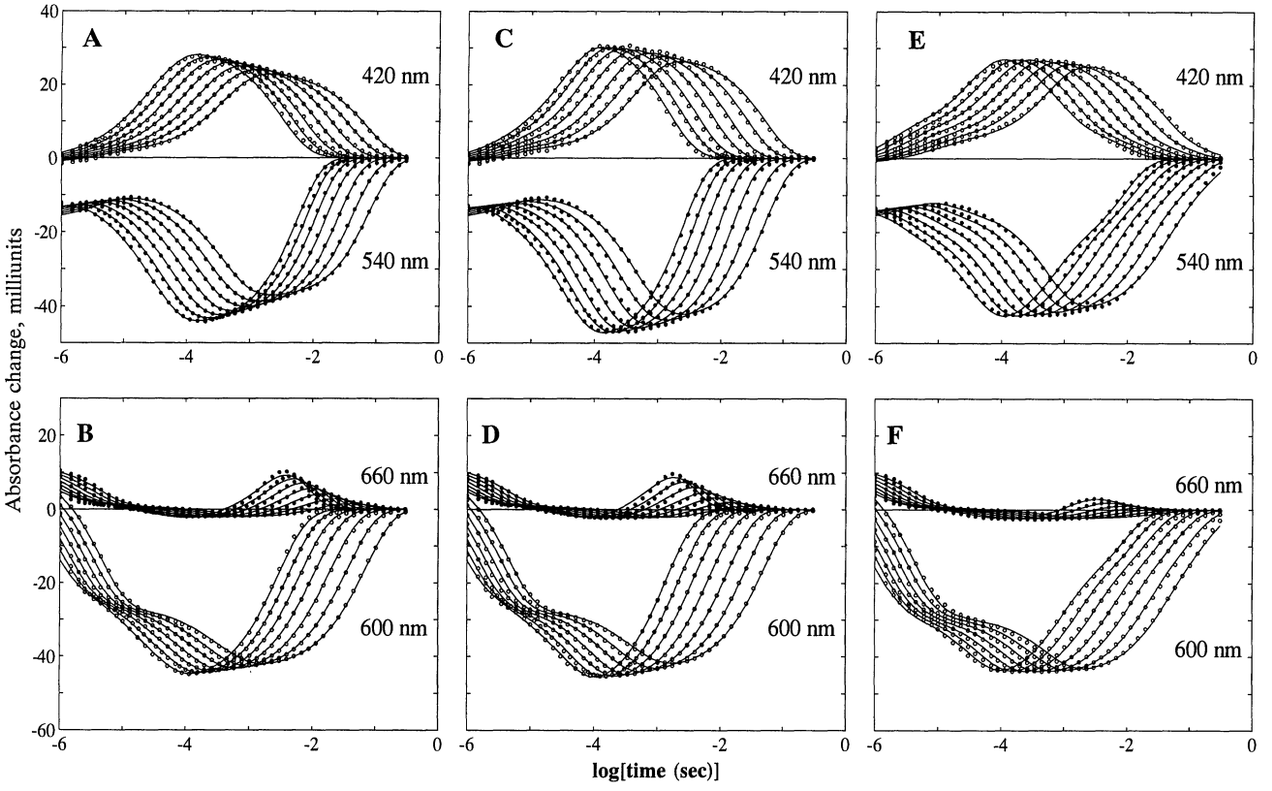

FIG. 1. Comparison of the experimental data and best-fit theoretical curves obtained using the model $K \rightleftharpoons L \rightleftharpoons X \rightleftharpoons M \rightleftharpoons N \rightleftharpoons O \rightarrow bR$ (Eq. 3). The data and fits are shown at pH 5 (*A* and *B*), pH 7 (*C* and *D*), and pH 9 (*E* and *F*) for four wavelengths (420, 540, 600, and 660 nm) and seven temperatures (5°C–35°C in 5°C steps). In each panel, the experimental data at the shorter wavelength are denoted by the open circles, and those at the longer wavelength are denoted by filled circles. The standard deviation of the fit, defined as the square root of the sum of squared deviations between fit and data divided by $(n - p)$, where n is the number of data points and p is the number of parameters varied (18, 19), is 4.07×10^{-4} absorbance units.

N and O, is highly dependent on both pH and temperature. At pH 9, the principal intermediate in the decay pathway is N, which exhibits nearly temperature-independent populations of approximately 60% of the fraction cycling. The temperature dependence of the O population is a striking feature of the fits at both pH 5 and pH 7. It is only at temperatures of 20°C and above that O becomes a major intermediate in the cycle. The population of this intermediate is largest (≈45%) at pH 5 and 35°C. The re-formation of bR is slowest at pH 9 and fastest at pH 7. The very small O populations found at pH 9 suggest that it is the slow formation of the O intermediate that limits the re-formation of bR.

The difference spectra between each intermediate and bR produced by the fit, as well as the absolute spectra obtained by adding a bR spectrum, scaled by the fraction cycling, to the difference spectra, are shown in Fig. 3. The spectrum of the K intermediate is in good agreement with those measured with higher time resolution (23), and the spectra of the L and N intermediates are also similar to those previously published (4, 5, 23, 24) except that a shoulder on the long wavelength side of the L spectrum is significantly decreased by allowing a back-reaction from L to K in the model. The difference spectra of both the X and M intermediates exhibit peaks near 410 nm arguing that both contain the 13-cis deprotonated chromophore.

By using a single value for the fraction cycling, it is not possible to calculate absorption spectra for all the intermediates that exhibit a single absorption band in the visible region and extinction coefficients that are positive at all wavelengths (cf. ref. 25) from the difference spectra in Fig. 3*A*. To avoid negative extinctions, the spectra of the M and X intermediates must both exhibit two absorption bands, one peaking near 410 nm and the other near 560 nm. [A second peak on the long wavelength side of the 420 nm peak was also seen in previous analyses (4, 25).] The deprotonated 13-cis M intermediate trapped at low temperature, high pH, and high light intensity exhibits no green peak in its spectrum (26). The fit has therefore included species in which the chromophore remains protonated in the states described as X and M in Eq. 3. Although this result helps to resolve a discrepancy between the concentrations of the M intermediate in Fig. 2 and time-resolved resonance Raman data, which suggest that the maximum population of the deprotonated, 13-cis intermediate is only about 40% of the cycled chromophores at neutral pH (9, 14), it strongly suggests that the present model does not represent a complete description of the photocycle with respect to these intermediates. We also note that the peak of the spectrum of the O intermediate is observed at about 580 nm, significantly to the blue of previous estimates (4, 25), which have placed the peak near 640 nm. The peak is at nearly the same wavelength as the peak of the K intermediate, but the band is considerably broader.

Based on these results, we conclude that the fully reversible six-intermediate model (Eq. 3) is *not* a complete description of the photocycle kinetics. In marked contrast to this conclusion, Varo and Lanyi (16, 17) have recently reported that time-resolved absorption spectra collected at pH 7 for bR and its Asp-96 → Arg mutant in purple membrane and in detergent micelles could be fitted using the six-intermediate model

$$K \rightleftharpoons L \rightleftharpoons M_1 \rightharpoonup M_2 \rightleftharpoons N \rightleftharpoons O. \qquad [4]$$
$$\searrow \quad \swarrow$$
$$bR$$

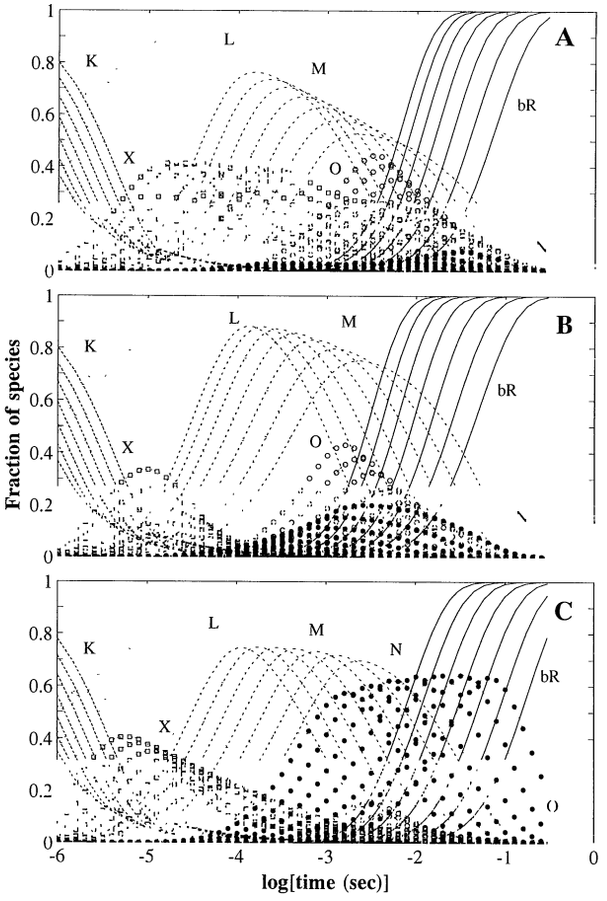

FIG. 2. Time dependence of the species populations of the K ⇌ L ⇌ X ⇌ M ⇌ N ⇌ O → bR kinetic model (Eq. 3). The results are shown at seven temperatures (5°C–35°C in 5°C steps from right to left) for pH 5 (*A*), pH 7 (*B*), and pH 9 (*C*). The species are denoted as follows: - - - -, K; ·····, L; ···□···□···□···, X; -·-·-·-, M; ···●···●···●···, N; ···○···○···○···, O; ——, bR.

With the exception of the N → bR branch, this model is a special case of Eq. 3. Their analysis begins with the selection of a set of spectra for the intermediate species that produce bandwidths and peak positions similar to those obtained in previous analyses. These spectra are then used to calculate the concentrations of intermediates, and the resulting kinetic traces are approximated by adjusting the rates of the model. We note that the selection of *five* or *six* basis spectra in terms of which to represent the data is necessarily imprecise (23) and imposes an irreversible bias on the resulting fit. The bypass reaction from N → bR in their model (Eq. 4), required by their choice of the spectrum for the O intermediate, is one example of such a bias. Moreover, their fits to the species concentrations appear significantly worse than the preliminary fits in which a subset of the data at a single pH was fitted by using a reversible model having only four intermediates. While the present analysis supports their analysis in requiring that *at least* six intermediates are necessary to describe the photocycle kinetics, our results suggest that the conclusion of these authors may be somewhat optimistic.

It is likely that the problems encountered in describing the appearance and decay of the deprotonated 13-cis Schiff base chromophore with the six-intermediate model (Eq. 3) arise because additional species, probably indistinguishable from those described in the original photocycle (Eq. 1) on the basis of their visible absorption spectra alone, are significantly occupied at some point in the cycle. A rapidly growing body of evidence, recently summarized by Henderson *et al.* (27)

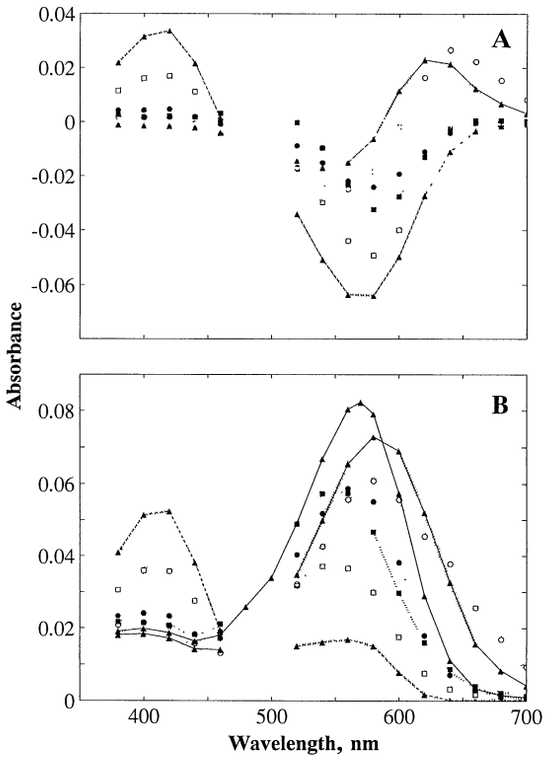

FIG. 3. Absorption spectra of the intermediates in the K ⇌ L ⇌ X ⇌ M ⇌ N ⇌ O → bR model (Eq. 3). (*A*) The difference spectra between each intermediate and bR obtained from the fit. (*B*) Absorption spectra obtained by adding back the bR spectrum of the fraction cycling (—▲—▲—; see text for details). The spectrum of each species is depicted as follows: —▲—▲—, K; ···■···■···■···, L; ···□···□···□···, X; -▲- -▲- -▲-, M; ···●···●···●···, N; ···○···○···○···, O. The dotted lines depict the errors in the determination of the spectra of these intermediates.

and Mathies *et al.* (28), exists for states that differ in the distribution of bound protons. These results suggest that the L → M transition of the original photocycle (4) involves at least two independent steps. These are (*i*) the transfer of a proton from the Schiff base to Asp-85 and (*ii*) the release of a different proton to the cell exterior. A sufficient explanation for the problems associated with the rise of the population of the deprotonated 13-cis chromophore, is that these two steps, while thermodynamically coupled, do not occur simultaneously. In this case, a minimal model for the early steps of the cycle requires at least two L intermediates in which the retinal is 13-cis and protonated and two M intermediates in which the retinal is 13-cis and deprotonated.

$$\begin{array}{ccccc} \text{K-H}^+ & \rightleftharpoons & \text{L-H}^+ & \rightleftharpoons & \text{M-H}^+ \\ & & \downarrow\uparrow \rightarrow \text{H}^+ & & \downarrow\uparrow \rightarrow \text{H}^+ \quad \text{cell exterior} \\ & & \text{L} & \rightleftharpoons & \text{M} \rightleftharpoons \text{N} \\ & & \text{cell interior} \quad \text{H}^+ \rightarrow \downarrow\uparrow & & \end{array} \qquad [5]$$

$$\text{N-H}^+ \rightleftharpoons \text{O-H}^+ \rightarrow \text{bR-H}^+$$

Additional proton binding steps and/or changes in local protein structure, such as the change in protein conformation proposed by the C-T model (6, 28), could introduce additional pairs of parallel states at other points in the cycle (29). One other pair, the protonated and unprotonated forms of the N intermediate, is included in Eq. 5 to explain the pH dependence of the N → O transition rates. In the second form

of the N intermediate, another residue on the interior side of the protein, tentatively identified as Asp-96, is protonated in addition to the 13-cis Schiff base chromophore (27, 28). The fit (Table 1) suggests that the reisomerization of the retinal to form the all-trans O intermediate and *not* the protonation of the Schiff base to form N is the critical proton-dependent step in the recovery of the light-adapted state. Ames and Mathies (14) have reached a similar conclusion from their analysis of time-resolved Raman data measured under high salt conditions. The presence of this additional intermediate between N and O can rationalize the difficulties encountered in modeling the rise of the O intermediate (Fig. 1) using the six-intermediate model (Eq. **3**).

In conclusion, we note that limitations imposed by the optical spectra make it unlikely that further details of the cycle can be resolved simply by fitting more accurate or more complete visible absorption data. To critically test models such as Eq. **5**, it will be necessary to include additional data that characterize other structural features of the molecule, such as the protonation states of individual residues and/or protein conformational states, and to fit this data simultaneously with visible absorption data. Recent results suggest that time-resolved Fourier-transform infrared measurements (30) will prove extremely useful in this regard. Initial efforts in this direction have included measurements of the kinetics of charge translocation from photocurrent measurements (31) and of proton release and uptake using indicators (32) but, to this point, no detailed modeling of these data has been reported.

We thank Drs. W. Stoeckenius, John Nagle, and Eric Henry for valuable discussions.

1. Stoeckenius, W. & Bogomolni, R. (1982) *Annu. Rev. Biochem.* **52,** 587–616.
2. Khorana, H. G. (1988) *J. Biol. Chem.* **263,** 7439–7442.
3. Birge, R. R. (1990) *Biochim. Biophys. Acta* **1016,** 293–327.
4. Lozier, R. H., Bogomolni, R. A. & Stoeckenius, W. (1975) *Biophys. J.* **15,** 955–962.
5. Kouyama, T., Nasuda-Kouyama, A., Ikegami, A., Mathew, M. K. & Stoeckenius, W. (1988) *Biochemistry* **27,** 5855–5863.
6. Fodor, S. P. A., Ames, J. B., Gebhard, R., van den Berg, E. M. M., Stoeckenius, W., Lugtenberg, J. & Mathies, R. A. (1988) *Biochemistry* **27,** 7097–7101.
7. Marcus, M. A. & Lewis, A. (1978) *Biochemistry* **17,** 4722–4735.
8. Korenstein, R., Hess, B. & Kuschmitz, D. (1978) *FEBS Lett.* **93,** 266–270.
9. Diller, R. & Stockburger, M. (1988) *Biochemistry* **27,** 7641–7651.
10. Nagle, J. F., Parodi, L. A. & Lozier, R. H. (1982) *Biophys. J.* **38,** 161–174.
11. Groma, G. I. & Dancshazy, Zs. (1986) *Biophys. J.* **50,** 357–366.
12. Parodi, L. A., Lozier, R. H., Bhattacharjee, S. M. & Nagle, J. F. (1984) *Photochem. Photobiol.* **40,** 501–512.
13. Otto, H., Marti, T., Holz, M., Mogi, T., Lindau, M., Khorana, H. G. & Heyn, M. P. (1989) *Proc. Natl. Acad. Sci. USA* **86,** 9228–9232.
14. Ames, J. B. & Mathies, R. A. (1990) *Biochemistry* **29,** 7181–7190.
15. Varo, G., Duschl, A. & Lanyi, J. K. (1990) *Biochemistry* **29,** 3798–3804.
16. Varo, G. & Lanyi, J. K. (1991) *Biochemistry* **20,** 5008–5015.
17. Varo, G. & Lanyi, J. K. (1991) *Biochemistry* **30,** 5015–5022.
18. Clore, G. M. & Chance, E. M. (1978) *Biochem. J.* **173,** 799–810.
19. Clore, G. M. (1983) in *Computing in Biological Sciences*, eds. Geisow, M. J. & Barrett, A. N. (Elsevier, New York), pp. 313–348.
20. Xie, A. H., Nagle, J. F. & Lozier, R. H. (1987) *Biophys. J.* **51,** 627–635.
21. Chance, E. M., Curtis, A. R., Jones, I. P. & Kirby, C. R. (1979) United Kingdom Atomic Energy Authority, Harwell (H. M. Stationery Office, London, U.K.), Rep. No. R-8775.
22. Hanomoto, J. H., Dupuis, P. & El-Sayed, M. A. (1984) *Proc. Natl. Acad. Sci. USA* **81,** 7083–7087.
23. Hofrichter, J., Henry, E. R. & Lozier, R. H. (1989) *Biophys. J.* **56,** 693–706.
24. Mauer, R., Vogel, J. & Schneider, S. (1987) *Photochem. Photobiol.* **46,** 255–262.
25. Nagle, J. F., Parodi, L. A. & Lozier, R. H. (1982) *Biophys. J.* **38,** 161–174.
26. Becher, B., Tokunaga, F. & Ebrey, T. G. (1978) *Biochemistry* **17,** 2293–2300.
27. Henderson, R., Baldwin, J. M., Ceska, T. A., Zemlin, F., Beckmann, E. & Downing, K. H. (1990) *J. Mol. Biol.* **213,** 899–929.
28. Mathies, R. A., Lin, S. W., Ames, J. B. & Pollard, W. T. (1991) *Annu. Rev. Biophys. Biophys. Chem.* **20,** 491–518.
29. Smith, S. O., Lugtenberg, J. & Mathies, R. A. (1985) *J. Membr. Biol.* **85,** 95–109.
30. Braiman, M. S., Bousché, O. & Rothschild, K. J. (1991) *Proc. Natl. Acad. Sci. USA* **88,** 2388–2392.
31. Holz, M., Lindau, M. & Heyn, M. P. (1988) *Biophys. J.* **53,** 623–633.
32. Otto, H., Marti, T., Holz, M., Mogi, T., Stern, L. J., Engel, F., Khorana, H. G. & Heyn, M. P. (1990) *Proc. Natl. Acad. Sci. USA* **87,** 1018–1022.